

Jets in coronal holes: Hinode observations and 3D computer modelling

F. Moreno-Insertis¹, K. Galsgaard², I. Ugarte-Urra³

ABSTRACT

Recent observations of coronal hole areas with the XRT and EIS instruments onboard the *Hinode* satellite have shown with unprecedented detail the launching of fast, hot jets away from the solar surface. In some cases these events coincide with episodes of flux emergence from beneath the photosphere. In this letter we show results of a 3D numerical experiment of flux emergence from the solar interior into a coronal hole and compare them with simultaneous XRT and EIS observations of a jet-launching event that accompanied the appearance of a bipolar region in MDI magnetograms. The magnetic skeleton and topology that result in the experiment bear a strong resemblance to linear force-free extrapolations of the *SOHO*/MDI magnetograms. A thin current sheet is formed at the boundary of the emerging plasma. A jet is launched upward along the open reconnected field lines with values of temperature, density and velocity in agreement with the XRT and EIS observations. Below the jet, a split-vault structure results with two chambers: a shrinking one containing the emerged field loops and a growing one with loops produced by the reconnection. The ongoing reconnection leads to a horizontal drift of the vault-and-jet structure. The timescales, velocities, and other plasma properties in the experiment are consistent with recent statistical studies of this type of events made with *Hinode* data.

Subject headings: Sun: X-rays — Sun: Magnetic fields — Sun: Corona

¹Instituto de Astrofísica de Canarias (IAC), 38200 La Laguna (Tenerife), Spain; fmi@iac.es

²Niels Bohr Institute, University of Copenhagen, Copenhagen, Denmark; kg@astro.ku.dk

³Space Science Division, Naval Research Laboratory, Washington DC 20375, USA; iugarte@ssd5.nrl.navy.mil

1. Introduction

X-ray jets in coronal holes are being observed with unprecedented quality by the instruments onboard the *Hinode* satellite, in particular the X-Ray Telescope (XRT) (Golub et al. 2007) and the Extreme UV Imaging Spectrometer (EIS) (Culhane et al. 2007). With their enhanced sensitivity and spatial resolution, those instruments have revealed that the frequency of jet formation is at least an order of magnitude greater than was thought previously (Cirtain et al. 2007). The new observations are leading to an in-depth revision of the statistics of jet properties (Shimojo et al. 1996; Savcheva et al. 2007). Sometimes, the formation of the jet is seen to occur simultaneously with an episode of flux emergence from the solar interior (e.g., Canfield et al. 1996; Jiang et al. 2007). In many XRT events, a brightening close to the surface is followed by enhanced emission in a region with an *inverted-Y* shape above the former (Fig. 1). The *tail* of the inverted *Y* coincides with a fast jet.

This kind of jets is most probably a consequence of the field line reconnection between the upcoming magnetic system and the open ambient field in the coronal hole, as originally suggested by theory and 2D numerical experiments (Heyvaerts et al. 1977; Yokoyama & Shibata 1996). In this letter, we analyze XRT and EIS observations of a jet in a coronal hole cospatial with a simultaneous flux emergence event observed with *SOHO*-MDI (Sec. 2). We study the magnetic topology using linear force-free extrapolations from the MDI data. We then present the results of a three-dimensional experiment of flux emergence into a region in the atmosphere with temperature, density and magnetic field values akin to those in a coronal hole (Sec. 3). We explain the resulting three-dimensional structure (geometry, topology, dynamics) and show the excellent overall agreement with the observations.

2. Observations

A large coronal hole was observed near disk center on March 10, 2007 by the *Hinode* satellite (Kosugi et al. 2007). We present EIS and XRT observations of a jet that appeared at 06:20 UTC at solar coordinates $(-25'', -115'')$ within the equatorial hole, at the same time as a magnetic bipole emerged at the photosphere (Fig. 2). A low-latitude event was chosen to facilitate the extrapolation and radial velocity measurement. The evolution of the jet was inspected using XRT 512×512 pixel images taken in the Open/Ti_poly filter combination at a cadence of 70 s. Spatial sampling is $1''$ per pixel. The EIS observations consisted of 30 s exposures in sit-and-stare mode with the $1'' \times 512''$ slit. Standard routines were used in the data processing. The alignment between both instruments was done via cross-correlation of North-South cross-sections of the X-ray images with the Fe XII emission along the EIS slit. Accuracy is down to between $1''$ and $2''$ in the N-S direction and less than $5''$ in the

E-W. For the analysis of the magnetic flux density we used full disk magnetograms from *SOHO*-MDI (Michelson Doppler Imager, Scherrer et al. 1995). Only magnetograms with a 96-min cadence were available at the time of the jet. The closest one in time (06:27 UTC) shows a newly emerged bipole under the location where the jet is formed. The magnetic flux density of the emerged polarities is in the range $(-70, 88) \text{ Mx cm}^{-2}$ [i.e., $(-7, 8.8) 10^{-7} \text{ Wb m}^{-2}$] with total fluxes of $\approx 1 \times 10^{19} \text{ Mx} = 1 \times 10^{11} \text{ Wb}$. The magnetic topology was determined with a linear force-free extrapolation method (see details in Ugarte-Urra et al. 2007) and reveals the existence of a coronal null point and a separatrix dome that encloses the connectivity domain of the newly emerged flux.

In the XRT images (as, e.g., in the top-left panel of Fig. 2), we first see the appearance of small coronal loops that connect the pre-existing dominant ambient positive flux to the newly emerged negative polarity. This is followed immediately by the formation of the jet, oppositely oriented and rooted in the positive flux, with the footpoints most likely located where the separatrix surface intersects the photosphere. The top-right panel of the figure shows the relationship of the loops and jet to the magnetic topology from the extrapolation. The bottom right panel shows a side view of the topology with four labeled connectivity domains. In region 1 lie the magnetic connections between the two newly emerged polarities. The loops on the XRT image correspond to region 3. A natural explanation for this configuration is that the emerging flux (region 1) is merging with flux from region 2 yielding two reconnected-line regions (3 and 4). The jet must be in an open-field region, so it must be in region 4, and close to the separatrix (dark-blue field lines). This is consistent with what the projected extrapolation and the XRT image suggest and is also in agreement with the results of the numerical simulation presented in Sec. 3. At least two consecutive jet events can be identified in the XRT movie before the loops grow and finally populate the whole enclosed domain. The initial and most impulsive phase lasts around 12 min.

The EIS slit crosses the jet structure at about $15''$ to the East side of its origin. EIS's unique combination of high spatial, spectral and temporal resolution can provide diagnostics for the density and velocity (for an in-depth discussion of previous EUV spectroscopic observations of jets see Wilhelm et al. 2002; Ko et al. 2005; Pike & Harrison 1997 and references therein). On the jet we measured (Fig. 2, bottom-left panel) a line-of-sight blue-shifted velocity of up to 240 km s^{-1} in the Fe XII 195.12-Å line. The zero value is given by an average profile in the quiet coronal hole. After averaging two pixels along the slit and two exposures, to increase the signal-to-noise ratio, and subtracting the background emission, we also obtained an estimate for the electron density through the line ratio Fe XII 195.1/186.9: $5.5 \times 10^9 \text{ cm}^{-3}$. The density estimate is consistent with a filling factor of ≈ 0.2 for the Fe XII 195.1Å column emission measure, assuming photospheric abundance (Grevesse et al. 2007), a temperature corresponding to the maximum in the ionization fractions (Mazzotta et al.

1998) and a column depth of 4.7 Mm, equal to the jet’s measured width. We used CHIANTI v5.2 (Landi et al. 2006) for the calculations.

3. Numerical experiment

The numerical results were obtained for a three-dimensional domain of size 34 Mm \times 38 Mm in the horizontal directions and 33 Mm in the vertical direction, z , 29 Mm of which are above the photosphere. For the unmagnetized hydrostatic background at time $t = 0$ we chose an adiabatic stratification in the solar interior and a domain at photospheric temperature in the first 2 Mm above the surface; above it, we have a steep temperature gradient mimicking the transition region and, finally, an isothermal ($T = 1.1 \times 10^6$ K) corona in the topmost 25 Mm (as in Fig. 1 of Archontis et al. 2004, but with a much larger vertical domain). In the main experiment described here, ρ_{top} , the initial coronal density at the top of the box, was 5×10^{-16} g cm $^{-3}$, equivalent to an atom number density of $\approx 2 \times 10^8$ cm $^{-3}$. The domain is endowed at time $t = 0$ with a uniform magnetic field contained in the xz plane of strength $B_{amb} = 10$ G = 10 mT and pointing 25° away from the vertical. This field is dynamically dominant in the corona [$\beta \approx O(10^{-2})$], whereas it is very weak ($\beta \gg 1$) in the solar interior. Density and field strength are adequate to simulate coronal holes (see Wilhelm 2006; Harvey & Recely 2002). To explore the parameter space, experiments have also been carried out for B_{amb} equal to 25 G and 5 G, for $\rho_{top} = 1.5 \times 10^{-14}$ g cm $^{-3}$, and for inclinations of 15° and 0° to the vertical. We solve the MHD equations and assume an ideal gas law, no radiation cooling, and no heat conduction. The system is solved using the staggered-grid MHD code of our previous experiments (Nordlund & Galsgaard 1997; see Archontis et al. 2004). The numerical grid is non-uniform in the vertical direction, with minimum resolution of 5.3 points per scale height (pps) in the photosphere (65 pps in the corona), and has $350 \times 322 \times 320$ nodes in the (x, y, z) directions.

The emergence process is initiated by including a twisted magnetic flux tube with axis along the y coordinate direction located 1.7 Mm below the photosphere and with maximum field strength 3.8 kG. The tube is endowed with buoyancy in its central part so that it rises and reaches the surface in about 15 min. The main features of these initial phases are as described in our previous experiments (e.g., Archontis et al. 2004, 2005). Once in the atmosphere, the rising plasma has a considerable magnetic pressure excess and expands in all directions, albeit preferentially horizontally, whereby it adopts a *helmet* shape protruding from the solar interior. The pressure of the ambient coronal field opposes the expansion and the emerged volume reaches a maximum size of about 8 Mm in height, 11 Mm in the x direction (i.e., transverse to the original tube axis) and 17 Mm in the y direction.

The expansion just described firmly presses against each other the magnetic field in the emerged volume and the ambient corona. The field in the rising plasma is twisted around the tube axis; hence, it is almost counteraligned with the coronal field on one of the sides of the emerging volume. A thin, elongated current sheet is thereby formed (blue isosurface in Fig. 3) that embraces that side of the volume, resembling those obtained by Archontis et al. (2005). Seen in a vertical cut, the sheet appears as a thin stripe (in red in Fig. 4, top panel) of Syrovatskii type. Reconnection takes place across the current sheet: the arch-like loops next to it inside the *helmet* merge with the open loops coming in from the other side of the sheet. Two regions of reconnected field result; at the thin edge at the top of the current sheet, a set of open field lines are ejected: that region is visible in Fig. 4 (top panel) as a vertical band of diffuse current perturbations. At the lower edge, closed coronal loops ensue.

High velocity outflows are ejected from the upper and lower edge of the current sheet. The outflow at the upper edge (Fig. 4, center) is roughly horizontal and reaches peak speeds around 400 km s^{-1} (of order the local Alfvén speed). Shortly after leaving the reconnection site, it is deflected into two secondary jets propagating upward and downward along the field lines, basically as described in 2D by Yokoyama & Shibata (1996). The upgoing branch attains vertical velocities above 200 km s^{-1} (Fig. 4, center). High temperature values are reached in the jets and in the reconnection site itself. At the peak of activity (Figs. 3 and 4), the $6.5 \times 10^6 \text{ K}$ isosurface (in pink in Fig. 3) extends over the current sheet and into the jet. Values as high as $3 \times 10^7 \text{ K}$ (reconnection site) and slightly above 10^7 K (jet) are reached (Fig. 4, bottom). The high-T regions have the shape of an inverted-Y on top of the emerged material (Figs. 3 and 4), not unlike those observed by *Hinode* (Fig. 1). The density of the jet at the peak of activity is about 10 times the density of the unperturbed corona.

As reconnection proceeds, a *double-chambered vault* structure of closed loops develops below the jet, visible below the blue stripe in Figs. 3 and 4 (center and bottom panels): in one of the chambers (*the emerged chamber*), coronal loops with the original connectivity are still present; in the other (*the reconnected chamber*), the new set of closed, high-T coronal loops are being stored. The whole system strongly resembles the topology obtained in Sect. 2 through extrapolation from MDI data. As time proceeds, the *emerged chamber* decreases in transverse size while the *reconnected chamber* grows to a size similar to the original emerged volume. There results an apparent sideways *drift* of the vault and of the jet in the direction toward the reconnected loops, with roughly 10 km s^{-1} drift speed. This may correspond to the drift discussed by Savcheva et al. (2007).

The main phase of reconnection with jet speeds above 100 km s^{-1} lasts around 7 min, followed by an extended phase with lower temperature and jet velocities, for a total duration of some 20 min. In the early stages of reconnection, in turn, we observe cool and dense

plasma being ejected from the reconnection site. At that stage, the high-density shell that covers the emerging plasma is being merged with the ambient coronal field. The resulting reconnected open field lines become loaded with high-density [$\rho \approx O(10^2 \rho_{top})$], low-T [$O(10^5)$ K] material (visible to the left of the hot jet in Fig. 4, bottom panel).

4. Discussion

In this letter we have shown that the inverted-Y shaped jets recently observed by *Hinode*/XRT in coronal holes are a natural consequence of the emergence of magnetic flux from below the surface and its interaction with the preexisting open field in the coronal hole. Flux emergence is a prime candidate to trigger reconnection and the consequent launching of jets along field lines in the corona, as proposed through theoretical or 2D numerical results (Heyvaerts et al. 1977; Yokoyama & Shibata 1996) and through 3D experiments of jet formation in a horizontally magnetized atmosphere (Archontis et al. 2005; Galsgaard et al. 2007). Our present 3D experiments had a field configuration and stratification parameters akin to those in a coronal hole. The match we obtain between the X-Ray, EUV and magnetogram data and the numerical results is highly satisfactory concerning overall geometry, topology of the magnetic field, and density, temperature and velocity of the plasma. Various basic features obtained through 2D vertical cuts in our experiments agree qualitatively with the results of Yokoyama & Shibata (1996), in spite of the differences in parameter values. Beyond all that, our experiments permit discerning for the first time the 3D geometry of this type of events.

A number of refinements must be implemented for a better test of the match of the present numerical results with the observations, like heat conduction or radiative cooling. Those improvements are being included into this research at present.

Financial support by the European Commission through the SOLAIRE Network (MTRN-CT-2006-035484) and by the Spanish Ministry of Education through project AYA2007-66502 is gratefully acknowledged, as are the computer resources, technical expertise and assistance provided by the MareNostrum (BSC/CNS, Spain) and LaPalma (IAC/RES, Spain) supercomputer installations. Support from the NASA/*Hinode* program and from the Velux foundation is also acknowledged. *Hinode* is a Japanese mission developed and launched by ISAS/JAXA, with NAOJ, NASA and STFC as partners, and co-operated with ESA and NSC. *SOHO* is a project of cooperation between ESA and NASA.

REFERENCES

- Archontis, V., Moreno-Insertis, F., Galsgaard, K., & Hood, A. 2005, *ApJ*, 635, 1299
- Archontis, V., Moreno-Insertis, F., Galsgaard, K., Hood, A., & O’Shea, E. 2004, *A&A*, 426, 1047
- Canfield, R. C., Reardon, K. P., Leka, K. D., Shibata, K., Yokoyama, T., & Shimojo, M. 1996, *ApJ*, 464, 1016
- Cirtain, J. W., Golub, L., Lundquist, L., & et al. 2007, *Science*, in press
- Culhane, J. L., Harra, L. K., James, A. M., & et al. 2007, *Sol. Phys.*, 243, 19
- Galsgaard, K., Archontis, V., Moreno-Insertis, F., & Hood, A. 2007, *ApJ*, 666, 516
- Golub, L., DeLuca, E., Austin, G., & et al. 2007, *Sol. Phys.*, 243, 63
- Grevesse, N., Asplund, M., & Sauval, A. J. 2007, *Space Science Reviews*, 130, 105
- Harvey, K. L. & Recely, F. 2002, *Sol. Phys.*, 211, 31
- Heyvaerts, J., Priest, E. R., & Rust, D. M. 1977, *ApJ*, 216, 123
- Jiang, Y. C., Chen, H. D., Li, K. J., Shen, Y. D., & Yang, L. H. 2007, *A&A*, 469, 331
- Ko, Y.-K., Raymond, J. C., Gibson, S. E., & et al. 2005, *ApJ*, 623, 519
- Kosugi, T., Matsuzaki, K., Sakao, T., & et al. 2007, *Sol. Phys.*, 243, 3
- Landi, E., Del Zanna, G., Young, P. R., Dere, K. P., Mason, H. E., & Landini, M. 2006, *ApJS*, 162, 261
- Mazzotta, P., Mazzitelli, G., Colafrancesco, S., & Vittorio, N. 1998, *A&AS*, 133, 403
- Nordlund, A. & Galsgaard, K. 1997, *Tech. Rep.*, Astron. Observ., Copenhagen Univ.
- Pike, C. D. & Harrison, R. A. 1997, *Sol. Phys.*, 175, 457
- Savcheva, A., Cirtain, J., DeLuca, E., & et al. 2007, Submitted to *PASJ*
- Scherrer, P. H., Bogart, R. S., Bush, R. I., & et al. 1995, *Sol. Phys.*, 162, 129
- Shimojo, M., Hashimoto, S., Shibata, K., Hirayama, T., Hudson, H. S., & Acton, L. W. 1996, *PASJ*, 48, 123

Ugarte-Urra, I., Warren, H. P., & Winebarger, A. R. 2007, *ApJ*, 662, 1293

Wilhelm, K. 2006, *A&A*, 455, 697

Wilhelm, K., Dammasch, I. E., & Hassler, D. M. 2002, *Ap&SS*, 282, 189

Yokoyama, T. & Shibata, K. 1996, *PASJ*, 48, 353

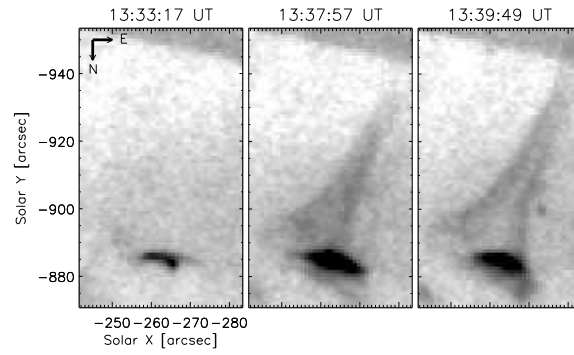


Fig. 1.— Polar coronal jet observed with XRT Al_{poly}/Open filter combination on the South coronal hole on January 20 2007. Color scale is reversed.

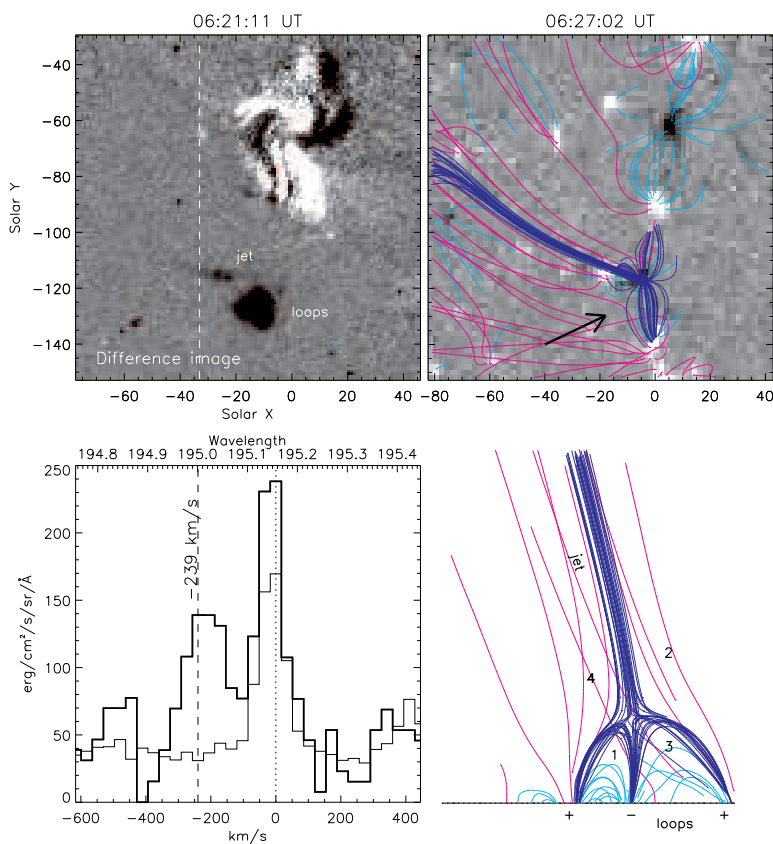


Fig. 2.— Coronal jet observed in an equatorial coronal hole on March 10 2007. Top left panel: difference XRT Open/Ti₂-poly image of the jet; the dashed line indicates the EIS slit position. Top right: MDI magnetogram and linear force free magnetic field extrapolation ($\alpha = -0.007 \text{ Mm}^{-1}$); the color code is: a) dark blue: field lines near the apparent magnetic null and the separatrices; b) light blue: field lines with two foot-points in the photosphere; c) red lines: open field lines. Bottom right: side view as indicated by the black arrow in the panel above. Numbers indicate connectivity regions. Bottom left: Fe XII 195.1 Å spectral profile at the jet location (thick line) at 06:21 UT. The thin line corresponds to an average profile elsewhere in the coronal hole.

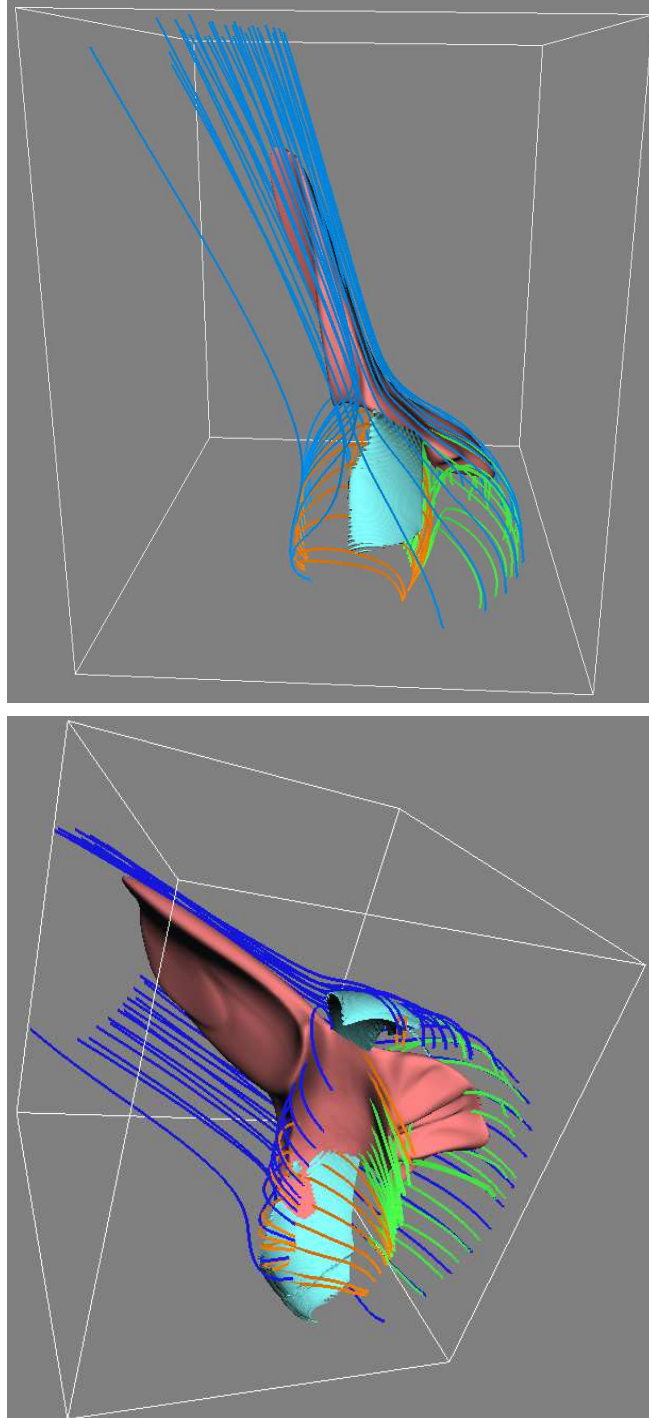


Fig. 3.— Three-dimensional view of the emerged region, the reconnection site and the jet at the time of peak reconnection activity (top: side view; bottom: view from below). The isosurface of j/B (in blue) delineates the collapsed current sheet on the side of the emerged volume. The temperature isosurface ($T = 6.5 \times 10^6$ K; in red) encompasses both the reconnection site and the jet volume. Underlying the jet and current sheet, a double set of current loops (emerged and reconnected, with field lines in orange and green, respectively) is visible, giving a 'double-chambered' vault shape to the region below the jet.

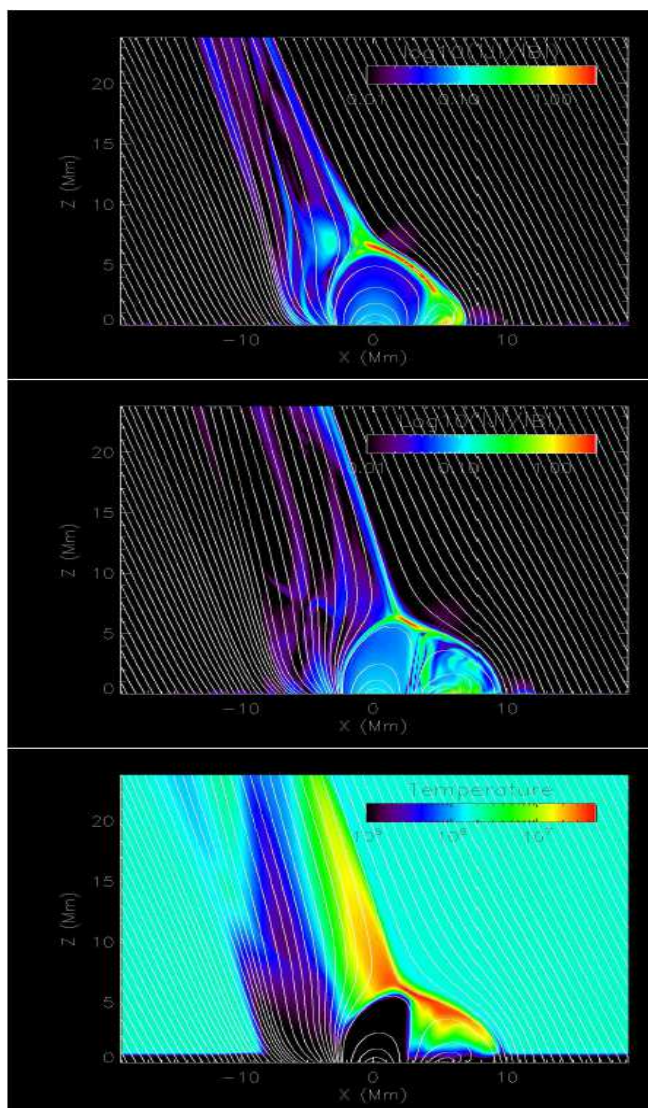


Fig. 4.— Vertical cuts at different stages of the evolution. Top: j/B distribution and field line projection at an early stage. A thin current sheet is situated to the top-right of the emerged coronal loops. The diffuse, elongated current perturbations to the top and left of the emerged volume correspond to previously reconnected field lines. Center: total velocity map and field line projection at the peak activity phase of the jet, occurring about 7 min later than the top panel. The double-chambered structure below the jet is clearly visible. Bottom: temperature distribution for the same snapshot as the central panel. An inverted-Y structure appears prominently, with $T \approx 3 \times 10^7$ K (reconnection site) and $\approx 10^7$ K (upward pointing jet).